Full paper

Applied Organometallic Chemistry

Received: 20 January 2016 Revised: 2 March 2016 Accepted: 8 March 2016 Published online in Wiley Online Library

(wileyonlinelibrary.com) DOI 10.1002/aoc.3484

Immobilization of Ru(terpyridine)(2,6-pyridinedicarboxylate) onto MCM-41 and its catalysis in the oxidation of alcohols

Yuecheng Zhang, Xiaochen Sun, Hongyu Zhang and Jiquan Zhao*

The ruthenium complex Ru(terpyridine)(2,6-pyridinedicarboxylate) was successfully grafted onto MCM-41 using a multi-step grafting method. The immobilized ruthenium complex was characterized thoroughly using Fourier transform infrared, Raman, UV–visible diffuse reflectance and energy-dispersive X-ray spectroscopies, X-ray diffraction, N_2 adsorption, scanning electron microscopy, thermogravimetric analysis and inductively coupled plasma analysis. This immobilized ruthenium complex showed excellent performance in the oxidation of various secondary alcohols to their corresponding ketones with *tert*-butyl hydroperoxide as oxidant under solvent-free conditions, and had the advantages of easy recovery and good reusability. Copyright © 2016 John Wiley & Sons, Ltd.

Additional supporting information may be found in the online version of this article at the publishers web site.

Keywords: Ru(terpyridine)(2,6-pyridinedicarboxylate); immobilization; oxidation; secondary alcohols; TBHP; MCM-41

Introduction

The oxidation of alcohols to their corresponding aldehydes and ketones is of crucial importance in organic chemistry because the obtained carbonyl compounds are widely used in the production of bulk and fine chemicals such as perfumes, pharmaceuticals and organic intermediates.[1–3] Classical methods to carry out this reaction are based on stoichiometric or even over-stoichiometric amounts of oxidants such as chromates,[4–7] manganese dioxide[8–10] and selenium dioxide,[11] which generate large amounts of byproducts and cause pollution to the environment. Therefore, it is highly necessary to develop catalytic oxidation processes for the oxidation of alcohols without using the traditional oxidants mentioned above. From both economic and environmental viewpoints, molecular oxygen is an ideal oxidant which generates water as the only byproduct in the oxidation process. Therefore, many catalytic systems based on stable nitroxyl radicals, such as 2,2,6,6-tetramethylpiperidine-1-oxyl (TEMPO), in combination with metals as co-catalysts have been developed.[12] However, most of these catalytic oxidation systems are inapplicable for the oxidation of secondary alcohols, or generally not suitable for large-scale applications. In addition to molecular oxygen, hydrogen peroxide and *tert*-butyl hydroperoxide (TBHP) are also regarded as environmentally benign oxidants. These oxidants in combination with transition metals or their complexes have been found to be very efficient in the oxidation of secondary alcohols to the corresponding ketones.[13–19]

In 2007, Beller and co-workers[20] applied Ru(terpyridine)(2,6-pyridinedicarboxylate) – Ru(terpy)(pydic) – to the oxidation of secondary alcohols to their corresponding ketones using hydrogen peroxide as oxidant. This complex showed excellent performance in the reaction in the absence of co-catalysts or organic solvents. Later, a similar ruthenium complex known as ruthenium bis (benzimidazole)(pyridinedicarboxylate) also proved to be very effective in the oxidation of secondary alcohols to ketones utilizing hydrogen peroxide as the oxidant.[21]

Although these ruthenium complexes performed well in the reaction, the difficult separation of the very expensive complexes from the reaction mixture makes them impossible to recycle directly. Heterogenization of these ruthenium complexes is expected to overcome this disadvantage. Therefore, we designed a method to immobilize Ru(terpy)(pydic) onto MCM-41. The immobilized ruthenium complex was evaluated in the oxidation of various alcohols to their carbonyl compounds. To our delight, this immobilized complex showed excellent catalytic activity and good recyclability in the oxidation of secondary alcohols with TBHP as oxidant under solvent-free conditions. Herein, we report the satisfactory results.

Experimental

Materials

4-Methylbenzaldehyde, 2-acetylpyridine, 2,6-pyridinedicarboxylic acid and TBHP (70%) were purchased from Energy Chemical, China. 3-Aminopropyltriethoxysilane, N-bromsuccinimide (NBS), α,α′-azoisobutyroniltrile (AIBN) and H_2O_2 (30%) were obtained from Tianjin Guangfu Fine Chemical Research Institute. Dichloro(*p*-cymene)ruthenium(II) dimer ($[Ru(p\text{-cymene})Cl_2]_2$) was purchased from Xi'an Kaili Chemical Company. MCM-41 was purchased from

* *Correspondence to: Jiquan Zhao, School of Chemical Engineering and Technology, Hebei University of Technology, Tianjin 300130, PR China. E-mail: zhaojq@hebut.edu.cn*

School of Chemical Engineering and Technology, Hebei University of Technology, Tianjin 300130, PR China

the Catalyst Plant of Nankai University, China. The secondary alcohols were obtained from Alfa Aesar China (Tianjin) Co. Ltd. Solvents were purified by standard methods and dried if necessary.

Characterization

^{1}H NMR spectra were recorded with tetramethylsilane as internal standard using a Bruker AC-P 400 type NMR spectrometer. Fourier transform infrared (FT-IR) spectra were recorded in the range 400–4000 cm^{-1} with a Bruker Vector 22 type instrument using KBr pellets. UV–visible diffuse reflectance spectra (UV-vis DRS) were obtained in the range 200–800 nm with a Varian Cary 300 UV–visible spectrophotometer. Powder X-ray diffraction (XRD) patterns were recorded using a Bruker X-ray diffractometer with D8 FOCUS lynx eye detector in the range of 2θ between 1° and 10° operating with a Cu anode at 40 kV and 40 mA. Analyses of surface area and pore structure were carried out using a Micromeritics ASAP2020M + C automated gas-sorption system, employing nitrogen as the adsorbate, after pretreatment of the sample at 120 °C for 10 h under reduced pressure. Scanning electron microscopy (SEM) and energy-dispersive X-ray spectroscopy (EDX) were carried out with a Nova Nano SEM450 instrument and an Octane Pro Det. The ruthenium content of the immobilized complex was analyzed using an X7 series inductively coupled plasma (ICP) mass spectrometer. Thermogravimetric analysis (TGA) was performed with an SDT/Q600 thermogravimetric analyzer at a temperature ranging from 20 to 800 °C with a temperature ramp of 10 °C min^{-1} under an air atmosphere. Raman spectra were measured at room temperature using an inVia Reflex visible Raman spectrometer in backscattering geometry equipped with excitation argon ion lasers working at 532 nm.

Catalyst preparation

*Synthesis of 4′-(p-methylphenyl)-2,2′:6′,2″-terpyridine (**1**)*

To a solution of 4-methylbenzaldehyde (19.4 g, 0.16 mol) and 2-acetylpyridine (37.8 g, 0.32 mol) in ethanol (300 ml) were added NaOH (12.2 g, 0.3 mol) and NH_4OH (460 ml, 25%) successively. The mixture was heated to 34 °C for 24 h, and then cooled to 20 °C. The off-white solid was collected by filtration and washed with ice-cold ethanol (60 ml). Recrystallization of the off-white solid from ethanol afforded white crystalline solid **1**. The characterization of **1** is shown in Fig. S1.

*Synthesis of 4′-(4-bromomethylphenyl)-[2,2′:6′,2″]terpyridine (**2**)*

A mixture of **1** (19.4 g, 0.06 mol), NBS (12.8 g, 0.07 mol) and AIBN (0.8 g, 0.005 mol) in dry CCl_4 (280 ml) was refluxed for 9 h. The warm reaction mixture was filtered to remove the succinimide byproduct, and the solvent was evaporated under vacuum. The crude product was recrystallized from ethanol–acetone (2:1) to afford **2** as a pale-yellow solid. The characterization of **2** is shown in Fig. S2.

Amino group-functionalized MCM-41

3-Aminopropyltriethoxysilane (2.6 ml, 0.01 mol) was slowly added to anhydrous toluene (300 ml) containing MCM-41 (8.0 g) under constant stirring and a nitrogen atmosphere at room temperature. The mixture was heated to reflux for 24 h. Then the solid product was filtered, washed with anhydrous ethanol and dried at 90 °C for 5 h to afford the amino group-functionalized material MCM-41-NH_2 (**B**).

*Preparation of MCM-41-NH-Terpy (**C**)*

In a typical process, **B** (7.5 g) and **2** (4.3 g, 0.01 mol) were dispersed in anhydrous toluene (120 ml) under a nitrogen atmosphere. The mixture was heated and refluxed for 10 h. Then the solid product was filtered, washed with anhydrous tetrahydrofuran and dried at 90 °C for 5 h to afford the terpy-functionalized MCM-41 (**C**).

*Preparation of immobilized ruthenium complex MCM-41-Ru (**D**)*

To a mixture of **C** (8.0 g) and [Ru(*p*-cymene)Cl_2]$_2$ (1.8 g, 0.003 mol) in methanol (90 ml) was added a solution of disodium pyridine-2,6-dicarboxylate (1.3 g, 0.006 mol) in methanol–water (2:1, 80 ml) under a nitrogen atmosphere. The mixture was heated to reflux for 5 h. The solid product was filtered, washed with methanol and water and dried at 90 °C for 5 h to afford **D**.

Typical procedure for oxidation of alcohols

A 5 ml two-necked round-bottom flask equipped with a magnetic stirrer was charged in succession with 0.02 g of **D** and 2 mmol of alcohol. The mixture was stirred and heated to 70 °C, and then 2.6 mmol of TBHP was added slowly at this temperature for 3 h. The progress of the reaction was monitored using GC with a PEG-20 M column. The product was purified by column chromatography over silica gel (*n*-hexane–ethyl acetate).

Results and discussion

Preparation of immobilized ruthenium complex D

The preparation route to **D** is shown in Scheme 1. First we synthesized 4′-(4-bromomethylphenyl)-[2,2′:6′,2″]terpyridine as described in the literature.[22] The ^{1}H NMR spectrum of the compound conforms to that in the literature.[22] After obtaining this compound, we began to immobilize the ruthenium complex onto MCM-41 using a multi-step grafting method. **B** was synthesized from MCM-41 and 3-aminopropyltriethoxysilane using a method previously reported by us.[23] In this process, the accessible silanol groups condensed with the triethoxysiloxane groups smoothly, which led to the attachment of a reactive terminal primary amine group to the surface of MCM-41.

In the process for preparing **C**, the amino group of **B** underwent a substitution reaction on the bromomethyl group of **2** smoothly to afford terpy-functionalized MCM-41 **C**. Using the same procedure for preparing Ru(terpy)(pydic) as in the literature,[24] the supported terpy ligand in combination with sodium 2,6-pyridinedicarboxylate coordinated with [Ru(*p*-cymene)Cl_2]$_2$ to give the immobilized ruthenium complex **D**.

The immobilized complex MCM-41-Ru was washed with methanol and water thoroughly to ensure the removal of substances absorbed on the outer surface of the support. The ruthenium content of the immobilized complex was determined using ICP analysis to be 1.93 wt%. Due to the washing procedure removing all absorbed substances from the MCM-41 surface, it is reasonable that the ruthenium content is from the complex attached onto MCM-41.

Characterization

FT-IR spectroscopy

FT-IR spectra of the samples are shown in Fig. 1. In all spectra the intense absorption band at 1081 cm^{-1} with a shoulder around 1200 cm^{-1} and those at 746 and 459 cm^{-1} are attributed to the

Applied Organometallic Chemistry

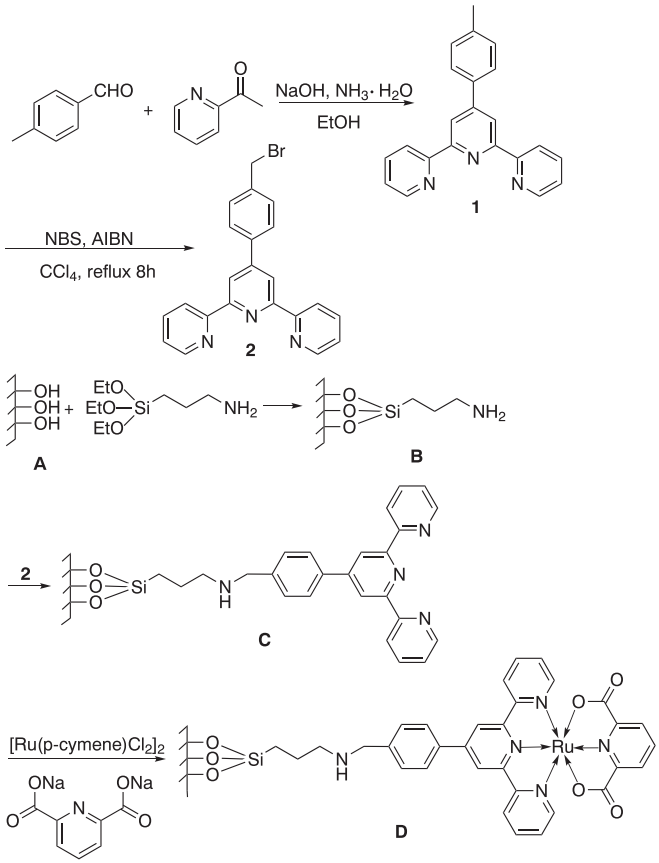

Scheme 1. Route for the synthesis of immobilized ruthenium complex.

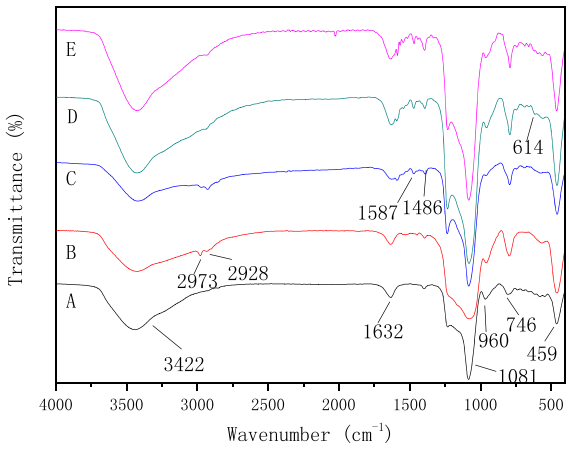

Figure 1. FT-IR spectra of MCM-41 (A), MCM-41-NH_2 (B), MCM-41-NH-Terpy (C), MCM-41-Ru (D), and used MCM-41-Ru (E).

Si–O–Si stretching and deformation vibrations, and the shoulder in particular is attributed to the porous nature of the MCM-41.[25,26] The band at 960 cm^{-1} in the spectrum of MCM-41 (**A**) is assigned to the bending vibration of Si–O–H,[27] and its intensity decreases with the modification of the wall of MCM-41 by triethoxysiloxane. The absorption bands at 3422 and 1632 cm^{-1} correspond to H–O–H bending vibrations of physisorbed water.[28] In the spectrum of MCM-41-NH_2 (**B**), the characteristic bands attributed to the stretching vibration of $-CH_2-$ can be seen around 2973 and 2928 cm^{-1}, which indicates that 3-aminopropyl group is attached successfully onto the wall of MCM-41. Compared with that of **B**, the spectrum of MCM-41-NH-Terpy (**C**) shows two additional bands at 1587 and 1486 cm^{-1}, attributed to the stretching vibration of C=N of the pyridine ring,[29] which indicates that the 4′-(*p*-methylenephenyl)-2,2′:6′,2″-terpyridine is successfully grafted onto the wall of MCM-41 through an iminepropyl chain. In the spectrum of MCM-41-Ru (**D**), a weak band at 614 cm^{-1} attributed to Ru–O vibration[30] is observed, indicating the formation of the immobilized complex. The used sample showed almost same spectrum compared with the fresh one, confirming that MCM-41-Ru is stable in a catalytic run.

Raman studies

Raman analysis was carried out to further confirm the formation of the immobilized complex. As shown in Fig. 2, the spectrum of MCM-41-Ru almost coincides with that of the homogeneous complex Ru(terpyridine)(2,6-pyridinedicarboxylate). In the spectra, the bands at 1607 and 1477 cm^{-1} are attributed to the stretching vibration of C=N from disodium pyridine-2,6-dicarboxylate,[29] and the bands at 1528 and 1356 cm^{-1} arise from the stretching vibration of C=N of terpyridine. The characteristic band at 644 cm^{-1} attributed to Ru–O vibration,[30] and the weak band at 458 cm^{-1} attributed to Ru–N vibration[30] are clearly observed in both spectra, indicating that the immobilized complex is successfully formed.

UV-vis DRS

Figure 3 shows the UV-vis DRS spectra following the synthesis procedure step by step. The spectra of MCM-41 (**A**) and MCM-41-NH_2 (**B**) exhibit no absorption bands above 300 nm. In the spectrum of MCM-41-NH-Terpy (**C**), band maxima at 214 and 290 nm are derived from the $\pi \rightarrow \pi^*$ transitions of phenyl and C=N groups[31]; and the band around 578 nm is from $n \rightarrow \pi^*$ of C=N in the conjugation system. In the spectrum of MCM-41-Ru (**D**), band at 510 nm is attributed to the d–d transition between Ru and ligands.[32] The result of UV-vis DRS is consistent with that of FT-IR spectra.

XRD analysis

The XRD pattern of MCM-41 (Fig. 4) exhibits three peaks in the 2θ range of 2–8° corresponding to the d100, d110 and d200 reflections of a regular hexagonal array of pores.[33] The patterns of MCM-41-NH_2 (**B**) and MCM-41-NH-Terpy (**C**) have no significant change

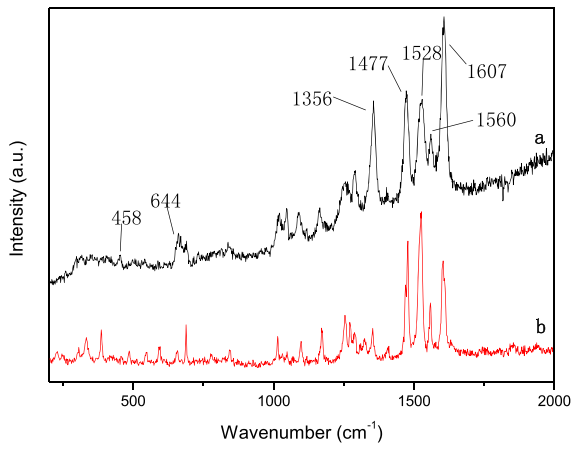

Figure 2. Raman spectra of MCM-41-Ru (a) and Ru(terpyridine)(2,6-pyridinedicarboxylate) (b).

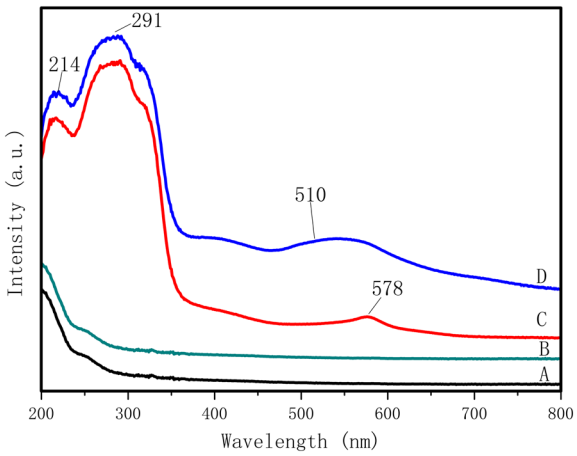

Figure 3. UV-vis DRS spectra of MCM-41 (A), MCM-41-NH_2 (B), MCM-41-NH-Terpy (C) and MCM-41-Ru (D).

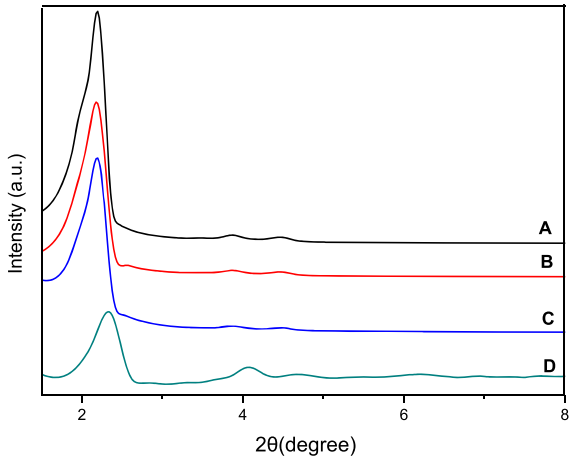

Figure 4. XRD analysis of MCM-41 (A), MCM-41-NH_2 (B), MCM-41-NH-Terpy (C) and MCM-41-Ru (D).

compared with that of MCM-41, which indicates that the MCM-41 framework structure remains after the multi-step grafting processes. A slight shift of the characteristic reflection to a higher angle and the obvious decrease of the intensity of the peak representing the d100 reflection are observed after the formation of the immobilized complex MCM-41-Ru (**D**), which may be ascribed to the partial structure collapse of parent MCM-41.[34]

Nitrogen adsorption

The BET surface area, pore size and pore volume of MCM-41, MCM-41 functionalized with each of amino and terpy, and the immobilized ruthenium complex are presented in Table 1. The surface area and pore volume of the samples decrease with the attachment of aminopropyl and terpy successively, and the formation of the immobilized complex. On the contrary, the pore diameter increases. The cooperative coordination of the supported terpy ligand and sodium 2,6-pyridinedicarboxylate with $[Ru(p\text{-cymene})Cl_2]_2$ to form the immobilized complex leads to a sharp decrease of surface area and pore volume. The surface area and pore volume of MCM-41-Ru are only 33.3 $m^2 g^{-1}$ and 0.1 $cm^3 g^{-1}$, respectively.

Table 1. BET surface area, pore volume and pore size of MCM-41, MCM-41-NH_2, MCM-41-NH-Terpy and MCM-41-Ru[a]

Entry	Sample	S_{BET} ($m^2 g^{-1}$)	Pore volume ($cm^3 g^{-1}$)	Pore diameter (nm)
1	MCM-41	1006.4	0.8	3.5
2	MCM-41-NH_2	781.6	0.6	3.2
3	MCM-41-NH-Terpy	281.7	0.2	3.0
4	MCM-41-Ru	33.3	0.1	11.8

[a]Pore size calculated using the BJH method.

SEM analysis

The SEM images of MCM-41 (**A**), MCM-41-NH_2 (**B**), MCM-41-NH-Terpy (**C**), MCM-41-Ru (**D**) and used MCM-41-Ru (**E**) are displayed in Fig. 5. The images reveal that all samples consist of many banana-like particles with particle size of about 800 × 300 nm, and the functionalized samples retain nearly the same morphology as that of the original MCM-41. These images indicate that the MCM-41 structure does not change largely during the ruthenium complex immobilization process. The same morphology of the used sample with that of the fresh MCM-41-Ru confirms that MCM-41-Ru is stable in a catalytic run. Meanwhile, EDX analysis was carried out and the results clearly illustrate the existence of Ru in the catalyst surface (Fig. 5(F)).

Thermal analysis

Figure 6 shows the TGA and DSC plots of MCM-41-Ru. The initial endothermic first stage occurs in the range 25 to 70 °C, with a weight loss of 5%, attributed to desorption of physisorbed water and other small molecules. The second stage lies between 300 and 450 °C, which corresponds to the pyrolytic endothermic degradation of the immobilized complex. A weight loss of 30% takes place in this stage. The results reveal that the immobilized Ru complex as a catalyst is stable during a catalytic run.

Catalytic properties of immobilized catalyst

The catalytic performance of MCM-41-Ru was evaluated for the oxidation of 1-phenylethanol as a model substrate with various oxidants. Molecular oxygen is the best oxidant from both economic and environmental viewpoints; therefore, we first tested molecular oxygen as oxidant in the oxidation of 1-phenylethanol. Almost no oxidation reaction takes place (Table 2, entry 1). Then hydrogen peroxide was tried, again due to its good performance in the oxidation of secondary alcohols catalyzed by Ru(terpy)(pydic).[20] Unexpectedly, very low conversion is obtained when 30% aqueous H_2O_2 is used as oxidant, and extending the reaction time has no significant effect on the reaction (Table 2, entries 2 and 4), which is very different from the same reaction catalyzed by homogeneous Ru(terpyridine)(2,6-pyridinedicarboxylate). It is difficult to tell what causes the large difference between the free and immobilized complex. Finally, we utilized TBHP as oxidant to carry out the reaction, and a delightful result was obtained. As evident from Table 2, a conversion of 99% with a selectivity of 99% toward acetophenone is obtained after 2.2 h at 70 °C (Table 2, entry 3).

Control experiments were performed to evaluate the necessity of the immobilized complex in the oxidation of 1-phenylethanol with TBHP as oxidant. As evident from Table 2, the use of the

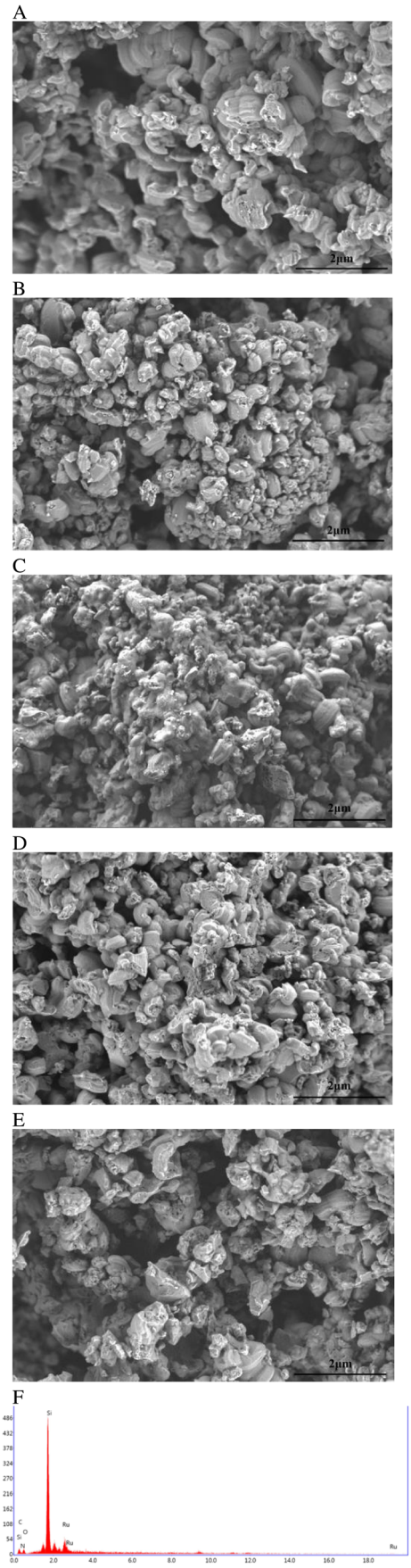

Figure 5. SEM images of MCM-41 (A), MCM-41-NH_2 (B), MCM-41-NH-Terpy (C), MCM-41-Ru (D) and used MCM-41-Ru (E). EDX analysis of MCM-41-Ru (F).

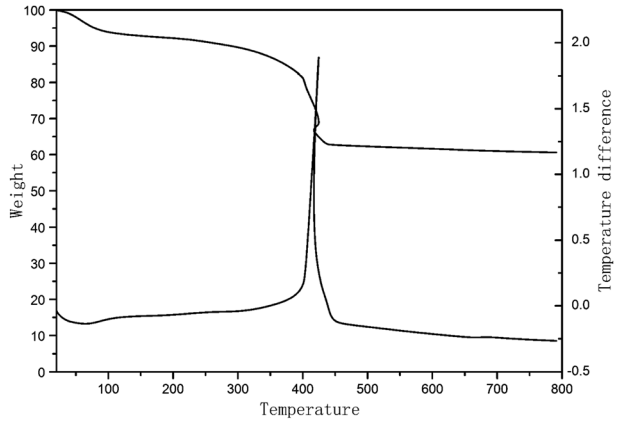

Figure 6. TGA and DSC curves of the thermal degradation of MCM-41-Ru.

Table 2. Selection of oxidant and necessity of the immobilized complex with 1-phenylethanol as model substrate[a]

Entry	Oxidant	Catalyst	Time (h)	Conv. (%)[b]	Select. (%)[b]	TON	TOF (h^{-1})
1	O_2	MCM-41-Ru	2.2	2.0	>99	10.5	4.8
2	H_2O_2	MCM-41-Ru	2.2	22.2	>99	116.8	53.1
3	TBHP	MCM-41-Ru	2.2	>99	>99	526.3	239.2
4	H_2O_2	MCM-41-Ru	5.5	23.2	>99	122.1	22.2
5	TBHP	—	2.2	28.4	>99	—	—
6	TBHP	MCM-41	2.2	29.0	>99	244.7	48.9
7	TBHP	MCM-41-NH_2	2.2	18.6	>99	182.6	36.5
8	TBHP	MCM-41-NH-Terpy	2.2	31.3	>99	185.3	37.0

[a]Reaction conditions: 1-phenylethanol (2 mmol), catalyst (0.02 g, 0.0038 mmol), oxidant (2.6 mmol), reaction temperature 70 °C.
[b]Determined by GC.

immobilized ruthenium complex is essential. Only 28.4% of 1-phenylethanol is converted to acetophenone in 2.2 h when no catalyst is added (Table 2, entry 5). When MCM-41, MCM-41-NH_2 and MCM-41-NH-Terpy instead of the immobilized ruthenium complex are used as catalysts respectively, the conversion of 1-phenylethanol is 29.0, 18.6 and 31.3% in 2.2 h (Table 2, entries 6–8).

The effect of MCM-41-Ru loading on the reaction was studied at 40 °C under the same conditions, and the results are shown in Table 3. When MCM-41-Ru loading is increased from 0.095 to 0.24 mol%, the time required to finish the reaction decreases from 12.5 to 5.0 h (Table 3, entries 1–4). Further increasing MCM-41-Ru loading does not increase reaction rate, but decreases it. This can be attributed to the direct decomposition of TBHP catalyzed by the over-loaded immobilized ruthenium complex.[35,36]

To obtain the optimal reaction conditions, the reaction temperature was examined. The results are listed in Table 4. It can be seen that the time to finish the reaction shortens with an increase of temperature from 40 to 70 °C, and the time to finish the reaction is only 2.2 h at 70 °C (Table 4, entries 1–4). An unfavorable result was obtained with a further increase of the reaction temperature. For instance, 1-phenylethanol is not completely converted to acetophenone when the temperature is 80 °C (Table 4, entry 5). This

Table 3. Effect of MCM-41-Ru loading on oxidation of 1-phenylethanol[a]

Entry	MCM-41-Ru (mol%)	Time (h)	Conv. (%)[b]	Select. (%)[b]	TON	TOF (h^{-1})
1	0.095	12.5	>99	>99	1052.6	84.2
2	0.14	8.0	>99	>99	714.3	89.2
3	0.19	5.5	>99	>99	526.3	95.7
4	0.24	5.0	>99	>99	416.7	83.3
5	0.28	5.5	>99	>99	357.1	64.9

[a]Reaction conditions: 1-phenylethanol (2 mmol), oxidant (6 mmol), reaction temperature 40 °C.
[b]Determined by GC.

Table 4. Effect of reaction temperature on oxidation of 1-phenylethanol[a]

Entry	Temperature (°C)	Time (h)	Conv. (%)[b]	Select. (%)[b]	TON	TOF (h^{-1})
1	40	25.0	88.3	>99	464.7	18.6
2	50	12.5	>99	>99	526.3	42.1
3	60	7.5	>99	>99	526.3	70.2
4	70	2.2	>99	>99	526.3	239.2
5	80	8.5	91.6	>99	482.1	56.7

[a]Reaction conditions: 1-phenylethanol (2 mmol), catalyst (0.02 g, 0.0038 mmol), oxidant (2.6 mmol).
[b]Determined by GC.

result is attributed to the decomposition of TBHP at higher temperature. Therefore, 70 °C was chosen as the reaction temperature in subsequent experiments.

The TBHP loading was optimized at 70 °C keeping the other parameters constant. Increasing the TBHP loading improves the reaction effectively. The results are listed in Table 5, from which it can be learned that the oxidation reaction could not finish at TBHP loading lower than or equal to 1:1.2. When the molar ratio of 1-phenylethanol to TBHP reaches 1:1.3, 1-phenylethanol is almost quantitatively converted to acetophenone in 2.2 h. Then the time to finish the reaction shortens with further increasing TBHP loading. Over-loading of TBHP will lead to unnecessary waste, thus the suitable molar ratio of 1-phenylethanol to TBHP is 1:1.3.

Table 5. Effect of TBHP loading on oxidation reaction of 1-phenylethanol[a]

Entry	Substrate:TBHP	Time (h)	Conv. (%)[b]	Select. (%)[b]	TON	TOF (h^{-1})
1	1:1.0	5.0	78.8	>99	414.7	82.9
2	1:1.1	5.0	88.6	>99	466.3	93.3
3	1:1.2	5.0	95.0	>99	500.0	100.0
4	1:1.3	2.2	>99	>99	526.3	239.2
5	1:1.4	1.8	>99	>99	526.3	292.4
6	1:1.5	1.5	>99	>99	526.3	350.9

[a]Reaction conditions: 1-phenylethanol (2 mmol), catalyst (0.02 g, 0.0038 mmol), temperature 70 °C.
[b]Determined by GC.

From the above experimental results we determined the optimal reaction conditions which are: 1-phenylethanol, 2 mmol; catalyst, 0.02 g (0.0038 mmol); TBHP, 2.6 mmol; reaction temperature, 70 °C. Under the optimal reaction conditions, 1-phenylethanol is almost quantitatively converted to acetophenone in 2.2 h in the absence of solvent.

Having determined the optimal conditions, the oxidation of various alcohols to their corresponding carbonyl compounds was explored under the optimal reaction conditions to evaluate the versatility of this novel catalytic system. As evident from Table 6, all secondary benzylic alcohols, including those bearing both electron-withdrawing and electron-donating groups, are selectively converted to their corresponding aromatic ketones in excellent yields (Table 6, entries 1–12). However, the time required to finish the reaction is much different. It seems that the catalytic system is more efficient for a substrate with an electron-withdrawing substituent (Table 6, entries 2–7). The position of the substituent on the benzene ring has obvious effects on the reactivity of secondary benzylic alcohols. A substrate with an *o*-substituent shows poor reactivity compared to that with an *m*- or *p*-substituent due to the steric hindrance (Table 6, entries 2–4, 7–9). Compared with their *p*- and *m*-isomers, high TBHP loading is required to get high yields in the cases of *o*-methyl-1-phenylethanol and *o*-chloro-1-phenylethanol as substrates (Table 6, entries 4 and 9). Overall, the reaction rate is determined by a combination of the electronic and steric effects. The immobilized ruthenium complex also shows high activity in oxidation of secondary aliphatic alcohols and cyclohexanol at high TBHP loading (Table 6, entries 13–15). These alcohols are generally difficult to oxidize using molecular oxygen catalyzed by copper/TEMPO-based catalysts.[37–40] However, the catalytic oxidation system does not work well with menthol due to large steric hindrance present in the structure (Table 6, entry 16).

The immobilized ruthenium complex was also applied to the oxidation of primary benzylic alcohols with TBHP as oxidant to see whether it was possible to obtain selectivity towards either the aldehyde or the carboxylic acid. Unfortunately, the selectivity is not controlled; only carboxylic acids as main products are obtained in all the cases (Table 6, entries 17–19). However, primary heterocyclic alcohols including 2-pyridylmethanol and 5-hydroxymethylfurfural are converted to their corresponding aldehydes in moderate yield at 40 °C (Table 6, entries 20 and 21); no deep oxidation products are observed in these cases. This may be due to the coordination of the heterocyclic atom to the Ru center, which decreased the activity of the immobilized ruthenium complex.

Recycling of catalyst

A recycle test was carried out under the optimal conditions determined as described above using 1-phenylethanol as a model substrate. After reaction, the catalyst was filtered, washed with methylene chloride, dried at 80 °C for 2 h and subjected directly to the next run. The results are summarized in Table 7. Comparing the results between the second and the first runs, the conversion decreases about 1.8%. With an increase of the number of recycles, the conversion of 1-phenylethanol decreases more and more (Table 7, entries 1–6). In the seventh run the conversion of 1-phenylethanol decreases to 75.6% (Table 7, entry 7), which is a reduction in activity of about 24.4% compared with that in the first catalytic run. To elucidate the reason, the ruthenium content of the catalyst after the seventh run was analyzed using ICP and is found to be 1.49%. The ruthenium loss is about 22.8% compared with that of the fresh catalyst, which agrees well with the activity

Table 6. Oxidation of various alcohols with TBHP catalyzed by MCM-41-Ru

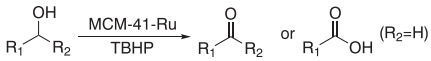

Entry	Substrate	Product	Time (h)	Conv. (%)[a]	Yield (%)[b]	Select. (%)[a]	TON	TOF (h^{-1})
1	1-Phenylethanol	Acetophenone	2.2	>99	88.1	>99	526.3	239.2
2[c]	1-(4-Methylphenyl)ethanol	4-Methylacetophenone	6.0	>99	92.8	>99	526.3	39.8
3	1-(3-Methylphenyl)ethanol	3-Methylacetophenone	8.0	>99	86.2	>99	526.3	65.8
4[e]	1-(2-Methylphenyl)ethanol	2-Methylacetophenone	5.5	>99	85.3	>99	526.3	95.7
5	1-(4-Fluorophenyl)ethanol	4-Fluoroacetophenone	3.2	>99	86.3	>99	526.3	164.4
6	1-(4-Bromophenyl)ethanol	4-Bromoacetophenone	4.0	>99	91.5	>99	526.3	131.5
7	1-(4-Chlorophenyl)ethanol	4-Chloroacetophenone	3.6	>99	88.0	>99	526.3	146.2
8	1-(3-Chlorophenyl)ethanol	3-Chloroacetophenone	5.0	>99	87.8	>99	526.3	105.3
9[d]	1-(2-Chlorophenyl)ethanol	2-Chloroacetophenone	8.0	>99	90.0	97.6	526.3	65.8
10[f]	1-Phenyl-1-propanol	1-Phenyl-1-propanone	6.0	>99	85.3	>99	526.3	87.7
11[f]	1-Indanol	1-Indanone	4.3	>99	89.6	>99	526.3	122.4
12	Benzhydrol	Benzophenone	3.3	>99	94.4	>99	526.3	159.5
13[e]	Cyclohexanol	Cyclohexanone	8.0	>99	90.1	>99	526.3	65.8
14[g]	2-Octanol	2-Octanone	13.0	94.2	85.3	>99	495.8	38.1
15[e]	1-Cyclohexyl-1-propanol	Cyclohexyl ethyl ketone	9.0	>99	89.1	>99	526.3	58.5
16	D,L-Menthol	Menthone	5.5	37.3	33.9	>99	196.3	35.7
17[h]	Benzyl alcohol	Benzoic acid	7.0	>99	78.0	85.3	526.3	75.2
18[e]	2-Chlorobenzenemethanol	2-Chlorobenzoic acid	9.8	>99	75.0	83.3	526.3	90.7
19[h]	4-Chlorobenzenemethanol	4-Chlorobenzoic acid	8.2	>99	73.3	80.9	526.3	64.2
20[i]	2-Pyridinemethanol	2-Pyridinecarboxaldehyde	16.0	58.0	41.5	98.2	305.2	19.0
21[i]	2-Thiophenemethanol	2-Thenaldehyde	7.0	74.0	52.9	98.6	389.4	55.6

Reaction conditions: 1-phenylethanol (2 mmol), catalyst (0.02 g, 0.0038 mmol), oxidant (2.6 mmol), temperature 70 °C.
[a]Determined by GC.
[b]Isolated yield.
[c]Oxidant: 2.8 mmol.
[d]Oxidant: 7.6 mmol.
[e]Oxidant: 5.8 mmol.
[f]Oxidant: 3.2 mmol.
[g]Oxidant: 5.2 mmol.
[h]Oxidant: 4.6 mmol.
[i]Oxidant: 6.0 mmol, temperature 40 °C.

Table 7. Recycle test of MCM-41-Ru for oxidation of 1-phenylethanol[a]

Entry	Run number	Conversion (%)[b]	Selectivity (%)[b]
1	1	>99	>99
2	2	97.2	>99
3	3	95.1	>99
4	4	91.0	>99
5	5	84.1	>99
6	6	78.6	>99
7	7	75.6	>99

[a]Reaction conditions: 1-phenylethanol (40 mmol), catalyst (0.4 g, 0.076 mmol), oxidant (52 mmol), temperature 70 °C, reaction time 2.2 h.
[b]Determined by GC.

reduction of the immobilized ruthenium complex. These results indicate that the deactivation of the immobilized ruthenium complex is mainly due to the leaching of ruthenium during the catalytic runs. Anyway, this immobilized ruthenium catalyst can be recycled four times without a large reduction of its activity.

Conclusions

The ruthenium complex Ru(terpyridine)(2,6-pyridinedicarboxylate) was successfully grafted onto MCM-41 using a multi-step grafting method. This immobilized ruthenium showed excellent performance in the oxidation of various secondary alcohols to the corresponding ketones with TBHP as an oxidant under solvent-free conditions. In addition, the immobilized complex also showed advantages of easy recovery and good recyclability. ICP analysis indicated that the slow deactivation of the immobilized ruthenium complex is mainly due to the leaching of ruthenium during the catalytic runs.

Acknowledgments

The authors are grateful for financial support from the National Natural Science Foundation of China (no. 21276061) and the Natural Science Foundation of Hebei Province, China (no. B2013202158).

References

[1] M. Hudlicky, *Oxidations in Organic Synthesis*, American Chemical Society, Washington, DC, **1990**.
[2] R. C. Larock, *Comprehensive Organic Transformations: A Guide to Functional Group Preparations*, Wiley-VCH, New York, **1999**.
[3] G. Tojo, M. Fernandez, *Oxidations of Alcohols to Aldehydes and Ketones: A Guide to Current Common Practice*, Springer, Boston, MA, **2006**.
[4] K. Bowden, I. M. Heilbron, E. R. H. Jones, B. C. L. Weedon, *J. Chem. Soc.* **1946**, 39–45.
[5] E. J. Corey, J. W. Suggs, *Tetrahedron Lett.* **1975**, *16*, 2647–2650.
[6] G. Piancatelli, A. Scettri, M. D'Auria, , Synthesis, **1982**, 245–258.
[7] F. A. Luzzio, F. S. Guziec, *Org. Prep. Proced. Int.* **1988**, *20*, 533–584.
[8] J. W. Ladbury, C. F. Cullis, *Chem. Rev.* **1958**, *58*, 403–438.
[9] A. J. Fatiadi, *Synthesis* **1976**, 133–166.
[10] R. J. K. Taylor, M. Reid, J. Foot, S. A. Raw, *Acc. Chem. Res.* **2005**, *38*, 851–869.
[11] J. March, *Advanced Organic Chemistry: Reaction, Mechanisms and Structure*, John Wiley, New York, **1992**.
[12] Q. Cao, L. M. Dornan, L. Rogan, N. L. Hughes, M. J. Muldoon, *Chem. Commun.* **2014**, *50*, 4524–4543.
[13] M. R. Maurya, N. Saini, F. Avecilla, *Inorg. Chim. Acta* **2015**, *438*, 168–178.
[14] G. D. Yadav, A. R. Yadav, *J. Mol. Catal. A* **2013**, *380*, 70–77.
[15] G. Sarmah, S. K. Bharadwaj, A. Dewan, A. Gogoi, U. Bora, *Tetrahedron Lett.* **2014**, *55*, 5029–5032.
[16] J. K. Mobley, M. Crocker, *RSC Adv.* **2015**, *5*, 65780–65797.
[17] M. Lenze, E. B. Bauer, *Chem. Commun.* **2013**, *49*, 5889–5891.
[18] B. M. Peterson, M. E. Herried, R. L. Neve, R. W. McGaff, *Dalton Trans.* **2014**, *43*, 17899–17903.
[19] H. B. Ji, Q. L. Yuan, X. T. Zhou, L. X. Pei, L. F. Wang, *Bioorg. Med. Chem. Lett.* **2007**, *17*, 6364–6368.
[20] F. Shi, M. K. Tse, M. Beller, *Chem. Asian J.* **2007**, *2*, 411–415.
[21] X. T. Zhou, H. B. Ji, S. G. Liu, *Tetrahedron Lett.* **2013**, *54*, 3882–3885.
[22] B. Tang, F. B. Yu, P. Li, L. L. Tong, X. Duan, T. Xie, X. Wang, *J. Am. Chem. Soc.* **2009**, *131*, 3016–3023.
[23] Y. R. Zhang, J. Q. Zhao, L. Q. He, D. M. Zhao, S. M. Zhang, *Micropor. Mesopor. Mater.* **2006**, *94*, 159–165.
[24] H. Nishiyama, Y. Motoyama, *Chem. Commun.* **1997**, 1863–1864.
[25] E. I. Kamitsos, A. P. Patsis, G. Kordas, *Phys. Rev. B* **1993**, *48*, 12499–12505.
[26] V. Caps, S. C. Tsang, *Appl. Catal. A* **2003**, *248*, 19–31.
[27] I. A. Rahman, P. Vejayakumaran, C. S. Sipaut, J. Ismail, M. Abu Bakar, R. Adnan, C. K. Chee, *Colloids Surf. A* **2007**, *294*, 102–110.
[28] M. R. Maurya, A. Kumar, J. Costa Pessoa, *Coord. Chem. Rev.* **2011**, *255*, 2315–2344.
[29] A. Patel, S. Singh, *Micropor. Mesopor. Mater.* **2014**, *195*, 240–249.
[30] Z. W. Yang, Q. X. Kang, F. Quan, Z. Q. Lei, *J. Mol. Catal. A* **2007**, *261*, 190–195.
[31] J. L. Wang, C. Wang, K. E. deKrafft, W. B. Lin, *ACS Catal.* **2012**, *2*, 417–424.
[32] M. Muthu Tamizh, K. Mereiter, K. Kirchner, R. Karvembu, *J. Organometal. Chem.* **2012**, *700*, 194–201.
[33] X. B. Dong, D. J. Wang, K. B. Li, Y. Z. Zhen, H. M. Hu, G. L. Xue, *Mater. Res. Bull.* **2014**, *57*, 210–220.
[34] D. Prava Sahoo, D. Rath, B. Nanda, K. M. Parida, *RSC Adv.* **2015**, *5*, 83707–83724.
[35] K. M. Tse, H. J. Jiao, G. Anilkumar, B. Bitterlich, F. Gadissa Gelalcha, M. Beller, *J. Organometal. Chem.* **2006**, *691*, 4419–4433.
[36] L. Qi, X. Y. Qi, L. L. Wang, L. L. Feng, S. Lu, *Catal. Commun.* **2014**, *49*, 6–9.
[37] S. F. Zhang, C. X. Miao, D. Q. Xu, W. Sun, C. G. Xia, *Chin. J. Catal.* **2014**, *35*, 1864–1873.
[38] Z. Lu, T. Ladrak, O. Roubeau, J. V. Toorn, S. J. Teat, C. Massera, P. Gamez, J. Reedijk, *Dalton Trans.* **2009**, 3559–3570.
[39] O. Das, T. K. Paine, *Dalton Trans.* **2012**, *41*, 11476–11481.
[40] P. Gamez, I. W. C. E. Arends, J. Reedijk, R. A. Sheldon, *Chem. Commun.* **2003**, 2414–2415.

Supporting Information

Additional supporting information may be found in the online version of this article at the publisher's web site.

Figure S1. ^{1}H NMR of 4′-(*p*-Methylphenyl)-2,2′:6′,2″-terpyridine
Figure S2. ^{1}H NMR of 4′-(4-Bromomethylphenyl)-[2,2′:6′,2″] terpyridine
Figure S3. ^{1}H NMR of acetophenone ($CDCl_3$) (Table 6, entry 1)
Figure S4. ^{1}H NMR of 4-Methylacetophenone ($CDCl_3$) (Table 6, entry 2)
Figure S5. ^{1}H NMR of 3-Methylacetophenone ($CDCl_3$) (Table 6, entry 3)
Figure S6. ^{1}H NMR of 2-Methylacetophenone ($CDCl_3$) (Table 6, entry 4)
Figure S7. ^{1}H NMR of 4-Fluoroacetophenone ($CDCl_3$) (Table 6, entry 5)
Figure S8. ^{1}H NMR of 4-Bromoacetophenone ($CDCl_3$) (Table 6, entry 6)
Figure S9. ^{1}H NMR of 4-Chloroacetophenone ($(CD_3)_2SO$) (Table 6, entry 7)
Figure S10. ^{1}H NMR of 3-Chloroacetophenone ($CDCl_3$) (Table 6, entry 8)
Figure S11. ^{1}H NMR of 2-Chloroacetophenone ($CDCl_3$) (Table 6, entry 9)
Figure S12. ^{1}H NMR of 1-Phenyl-1-propanone ($CDCl_3$) (Table 6, entry 10)
Figure S13. ^{1}H NMR of 1-Indanone ($CDCl_3$) (Table 6, entry 11)
Figure S14. ^{1}H NMR of benzophenone ($CDCl_3$) (Table 6, entry 12)
Figure S15. ^{1}H NMR of cyclohexanone ($CDCl_3$) (Table 6, entry 13)
Figure S16. ^{1}H NMR of 2-Octanone ($CDCl_3$) (Table 6, entry 14)
Figure S17. ^{1}H NMR of cyclohexyl ethyl ketone ($CDCl_3$) (Table 6, entry 15)
Figure S18. ^{1}H NMR of menthone ($CDCl_3$) (Table 6, entry 16)
Figure S19. ^{1}H NMR of benzoic acid ($CDCl_3$) (Table 6, entry 17)
Figure S20. ^{1}H NMR of 2-Chlorobenzoic Acid ($(CD_3)_2SO$) (Table 6, entry 18)
Figure S21. ^{1}H NMR of 4-Chlorobenzoic Acid ($(CD_3)_2SO$) (Table 6, entry 19)
Figure S22. ^{1}H NMR of 2-Pyridinecarboxaldehyde ($CDCl_3$) (Table 6, entry 20)
Figure S23. ^{1}H NMR of 2-Thenaldehyde ($CDCl_3$) (Table 6, entry 21)